Chemosphere 363 (2024) 142950

Contents lists available at ScienceDirect

Chemosphere

journal homepage: www.elsevier.com/locate/chemosphere

Environmentally persistent free radicals and other paramagnetic species in wildland-urban interface fire ashes

Mahbub Alam [a], James D. Sitter [b], Aaron K. Vannucci [b], Jackson P. Webster [c], Sandrine J. Matiasek [d], Charles N. Alpers [e], Mohammed Baalousha [a,*]

[a] Center for Environmental Nanoscience and Risk, Department of Environmental Health Sciences, Arnold School of Public Health, University of South Carolina, Columbia, SC, United States
[b] Department of Chemistry and Biochemistry, University of South Carolina, Columbia, SC, United States
[c] Department of Civil Engineering, California State University Chico, 400 W 1st St, Chico, CA, 95929, United States
[d] Department of Earth and Environmental Sciences, California State University Chico, 400 W 1st St, Chico, CA, 95929, United States
[e] U.S. Geological Survey, California Water Science Center, 6000 J Street, Sacramento, CA, United States

HIGHLIGHTS

- Paramagnetic species were measured in wildland-urban interface fire ash.
- The concentrations of EPFRs decreased with increased combustion completeness.
- The concentrations of EPFRs decreased with increased combustion completeness; black > gray > white.
- The concentration of isolated reduced Mn^{2+} ions increased with increased combustion completeness.
- WUI fire ash may be an important global source of EPFRs and reduced Mn^{2+}-bearing nanomaterials.

GRAPHICAL ABSTRACT

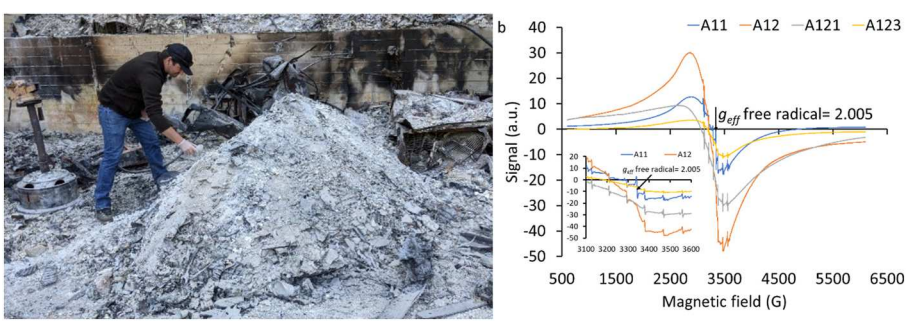

ARTICLE INFO

Handling editor: Petra Petra Krystek

Keywords:
Environmentally persistent free radicals
Electron paramagnetic resonance
Wildland-urban Interface fires
LNU Lightning Complex fire
North complex Fire

ABSTRACT

Wildland-urban interface (WUI) fires consume fuels, such as vegetation and structural materials, leaving behind ash composed primarily of pyrogenic carbon and metal oxides. However, there is currently limited understanding of the role of WUI fire ash from different sources as a source of paramagnetic species such as environmentally persistent free radicals (EPFRs) and transition metals in the environment. Electron paramagnetic resonance (EPR) was used to detect and quantify paramagnetic species, including organic persistent free radicals and transition metal spins, in fifty-three fire ash and soil samples collected following the North Complex Fire and the Sonoma-Lake-Napa Unit (LNU) Lightning Complex Fire, California, 2020. High concentrations of organic EPFRs (*e.g.*, 1.4×10^{14} to 1.9×10^{17} spins g^{-1}) were detected in the studied WUI fire ash along with other paramagnetic species such as iron and manganese oxides, as well as Fe^{3+} and Mn^{2+} ions. The mean concentrations of EPFRs in various ash types decreased following the order: vegetation ash ($1.1 \times 10^{17} \pm 1.1 \times 10^{17}$ spins g^{-1}) > structural ash ($1.6 \times 10^{16} \pm 3.7 \times 10^{16}$ spins g^{-1}) > vehicle ash ($6.4 \times 10^{15} \pm 8.6 \times 10^{15}$ spins g^{-1}) > soil ($3.2 \times 10^{15} \pm 3.7 \times 10^{15}$ spins g^{-1}). The mean concentrations of EPFRs decreased with increased combustion completeness indicated by ash color; black ($1.1 \times 10^{17} \pm 1.1 \times 10^{17}$ spins g^{-1}) > white ($2.5 \times 10^{16} \pm 4.4 \times 10^{16}$ spins g^{-1}) >

* Corresponding author.
E-mail address: mbaalous@mailbox.sc.edu (M. Baalousha).

https://doi.org/10.1016/j.chemosphere.2024.142950
Received 12 January 2024; Received in revised form 16 July 2024; Accepted 24 July 2024
Available online 26 July 2024

gray ($1.8 \times 10^{16} \pm 2.4 \times 10^{16}$ spins g^{-1}). In contrast, the relative amounts of reduced Mn^{2+} ions increased with increased combustion completeness. Thus, WUI fire ash is an important global source of EPFRs and reduced metal species (*e.g.,* Mn^{2+}). Further research is needed to underpin the formation, transformation, and environmental and human health impacts of these paramagnetic species in light of the projected increased frequency, size, and severity of WUI fires.

1. Environmental implication statement

This study highlights the role of wild-urban interface (WUI) fire ash as an important global source of environmentally persistent free radicals (EPFRs) and reduced transition metal species such as Mn^{2+}. The accumulation of EPFRs and reduced metals in WUI fire ash can be of social and environmental concern, impacting public health and safety, infrastructure, and contributing to land, water, and air pollution. Ash, and its associated contaminants, present public health risks to people (fire recovery workers, residents) and communities through direct and indirect ingestion, inhalation, and absorption. The mobilization of ashes by wind and water to receiving surface waters may pose risks to aquatic organisms.

2. Introduction

Fire (*i.e.,* wildfires, land management fires, and agricultural burns) is a frequent global phenomenon affecting 3–5 million square kilometers (km^2) annually around the world, burning ~ 4% of the Earth's vegetated land (Van Der Werf et al., 2017). Wildfire is also a frequent phenomenon across the United States, with more frequent fires of typically smaller areas in the eastern states than in western states (Wibbenmeyer and McDarris, 2021). For instance, in 2020, over 33,000 fires burned approximately 2,830 km^2 in the eastern states, while almost 26,000 wildfires burned 38,450 km^2 in the western states (Wibbenmeyer and McDarris, 2021). Wildfires have become increasingly destructive in recent years in the western United States, particularly in California, due to rising temperatures associated with climate change, preponderance of fuels resulting from long-term fire suppression, and a growing population living in proximity to wildland vegetation *i.e.,* at the wildland-urban interface (WUI) (Miller et al., 2009; Wibbenmeyer and McDarris, 2021; Williams et al., 2020). The area burned annually by wildfire across the United States has increased fivefold, from approximately 5,260 km^2 in 1983 to approximately 28,730 km^2 in 2021, with the 2020 fire season consuming a record 40,870 km^2 of wildland and destroying approximately 18,000 structures, including 9,600 homes (National Interagency Fire Center). Furthermore, it is estimated that over 2.0 million housing units, accounting for 15% of all housing units in California, and 6.9 million housing units in the United States are located in areas identified as having a high risk of burning in a wildfire event (Minott, 2017).

Fires consume fuels such as vegetation, structures, vehicles, *etc.*, leaving behind ash. Ash is the particulate residue after fire that remains *in situ*, is transported in air, or is deposited on the ground (Bodí et al., 2014). Ash produced by wildfires is a heterogeneous material composed primarily of oxides and hydroxides of base cations (*e.g.,* calcium (Ca^{2+}), magnesium (Mg^{2+}), and potassium (K^{+})) and metals (*e.g.,* iron and manganese oxides, FeOx, MnOx, *etc.*), and to a lesser extent, organic contaminants such as polycyclic aromatic hydrocarbons (Bodí et al., 2014; Burton et al., 2016). The makeup and color of fire ash depend on combustion completeness. Higher combustion completeness decreases the relative ash organic carbon content, increases the relative ash mineral content, and hence decreases the total mass of the ash (Bodí et al., 2014). Ash produced at lower combustion completeness is usually darker, coarser, and less dense than ash produced at higher combustion completeness (Bodí et al., 2014). Thus, black ash indicates low combustion completeness, gray ash indicates intermediate combustion completeness, and white ash indicates high combustion completeness (Bodí et al., 2014). Combustion processes also enrich metal(loid)s such as arsenic (As), cadmium (Cd), chromium (Cr), copper (Cu), iron (Fe), manganese (Mn), nickel (Ni), lead (Pb), and zinc (Zn) in ash (Burton et al., 2016; Campos et al., 2016; Parra et al., 1996; Plumlee et al., 2013; Wan et al., 2021) in the form of nanomaterials (Alam et al., 2023; Alshehri et al., 2023; Baalousha et al., 2022). During a fire, hydrocarbons present in fuels are converted to biochar or are oxidized to carbon monoxide, carbon dioxide, and water. Carbon oxidation results in the reduction of other species in the fuel, such as metal(loid)s. For instance, several studies demonstrated the reduction of iron oxides to magnetite (Fe_3O_4), wüstite (FeO), and zero-valent iron (Baalousha et al., 2022; Johnston et al., 2019) and of pentavalent arsenic (As(V)) to trivalent arsenic (As(III)) (Johnston et al., 2018, 2019), as well as the importance of organic matter in metal(loid) reduction.

In addition to these widely known components of ash, there is emerging evidence that ash may contain high amounts of environmentally persistent free radicals (EPFRs) (Sigmund et al., 2021). EPFRs are surface-bound organic compounds with unpaired electrons that can remain in the environment for durations ranging from minutes to years (Odinga et al., 2020; Sigmund et al., 2021). EPFRs are capable of generating reactive oxygen species, such as hydroxyl and superoxide radicals, responsible for inducing oxidative stress in living organisms (Liu et al., 2021; Odinga et al., 2020). In contrast to other free radicals with lifetimes in the range of microseconds to milliseconds, EPFRs are stable for prolonged periods of time (typically days to years), as they can bind to metal ion particle surfaces and become resonance-stabilized radicals (Sigmund et al., 2021; Vejerano et al., 2018). These characteristics make EPFRs highly susceptible to redistribution within the natural environment, with potential implications for environmental and human health (Jia et al., 2017; Liu et al., 2021; Odinga et al., 2020). Several studies reported the presence of EPFRs in human-derived pyrogenic material such as particulate matter from fossil fuel combustion (Saravia et al., 2013; Wang et al., 2018), biochar (Huang et al., 2020; Odinga et al., 2020; Ruan et al., 2019), and hydrothermal carbonization of sewage sludge (Zhu et al., 2019). However, to date, only one study reported measurements of EPFRs in materials associated with wildfire, mainly from vegetation ashes (Sigmund et al., 2021).

Electron paramagnetic resonance (EPR) spectroscopy is a method that specifically detects unpaired electrons and is therefore used to study molecular species containing paramagnetic centers such as organic radicals, transition metal ions (*e.g.,* trivalent iron and copper (Fe^{3+}, Cu^{3+}) and divalent manganese and copper (Mn^{2+}, Cu^{2+})) (Ayscough, 1967; Berliner and Reuben, 2012; Mabbs and Collison, 2013; Petrakis and Fraissard, 2012), and transition metal nanoparticles (*e.g.,* Fe_3O_4 and MnO_2) (Ivarsson et al., 2015; Kilias et al., 2020; Lee et al., 2011; Shames et al., 2019; Wang et al., 2013). Electron paramagnetic resonance techniques can provide information on oxidation state(s) of metals such as Mn, Fe, and Cu, their combination with other phases, and their structural environment (Mabbs and Collison, 2013).

The overall aim of this study is to investigate the nature of paramagnetic species in WUI fire ash using EPR and to determine the concentrations of EPFRs in WUI fire ash as a function of fuel source and combustion completeness.

3. Materials and methods

3.1. Sampling sites

Wildland-urban interface fire ash samples were collected from two

WUI fires that burned during the 2020 California fire season: the North Complex (NC) Fire and the Sonoma–Lake–Napa Unit (LNU) (a local unit of the California Department of Forestry and Fire Protection) Lightning Complex Fire (Fig. S1). A detailed description of these fires is given in previous publications (Alshehri et al., 2023; Baalousha et al., 2022). Briefly, the ***North Complex (NC) Fire*** was the seventh largest in California history and the second largest recorded in the northern Sierra Nevada. It burned 1,290 km^2 and destroyed 2,455 structures between August 17 and December 3, 2020. The distribution of burn severity within this fire was 2% low, 8% moderate, and 89% high (Fig. S1A) (inciweb, 2022; United States Department of Agriculture, 2020). Fire ash and soil samples were collected in the Berry Creek community, where most of the structures were destroyed (Fig. S2 and Table S1). ***The LNU Lightning Complex Fire***, the sixth largest in California history, burned 1,470 km^2 and destroyed 1,491 structures in Colusa, Lake, Napa, Solano, Sonoma, and Yolo Counties, approximately 60 km west of Sacramento, between August 17 and October 2, 2020 (CALFire, 2022). The distribution of burn severity within the fire perimeter was 12% low, 39% moderate, and 49% high (Fig. S1B). Fire ash samples were collected from vegetated areas and the built environment in Napa and Solano counties in the vicinity of Lake Berryessa (Fig. S3 and Table S1).

3.2. Sample collection

A total of fifty-three ash and soil samples were collected during October–November 2020 in the two fire-affected areas. In the LNU Lightning Complex Fire area, the collected ash samples include twenty-two structural, two vehicle, three mixed structural and vehicle, and four vegetation ashes. In the NC Fire area, the collected ash samples include four structural, three vehicle, and six vegetation ashes, along with eight soils affected by fire. In addition, a sample of air-fall ash was collected from a car's windshield located in the depositional zone of the NC Fire smoke plume (Table S1). Vegetation ash samples were collected from burned vegetation in forested areas far away from any human-made structures eliminating the potential contribution of structural and vehicle ashes to the vegetation ashes. Structural ash samples were collected from specific locations within burned residential structures and vehicle ash samples were collected from inside or underneath burned vehicles, minimizing the potential contribution of vegetation ashes to the collected structural and vehicle ashes. All samples were collected prior to any rain or other precipitation, stored in the dark, and were shipped in a plastic cooler to the University of South Carolina for further analysis.

Within the NC Fire area, ash and soil samples (Table S1) were collected from the community near Madrone Lake (Fig. S2B). When sampling burned structures in the NC Fire area, ash was collected from multiple locations within the footprint of the structure and subsamples were combined to form a representative composite sample. Note that sampling burned structures is very difficult because the ash is not uniform like vegetation ash. It is often a mixture of wallboard, insulation, and large debris, all mixed with combusted material residuals. In the burned vegetated areas, undisturbed ash was carefully scraped from the soil surface and collected to represent average (mixed) vegetation sources. To collect underlying soil, the area where surface ash was collected was carefully cleared of additional ash and the underlying soil was collected from two depths (0–2 cm and 10–15 cm) using a plastic scoop. All samples were collected in acid-washed high density polyethylene wide-mouth bottles.

Within the LNU Lightning Complex Fire area, undisturbed ash samples were collected from burned structures and vegetation to represent specific sources; ash samples were collected from multiple locations (*e.g.,* kitchen, living room, bedroom, garage, foundation, *etc.*) within each residential structure; detached structures adjacent to residences (*e.g.,* sheds, barns, and trailers) and a commercial structure (convenience store) were also sampled (Table S1, Fig. S3). Ash samples were collected with disposable plastic scoops and placed into zippered plastic bags.

All ash and soil samples were homogenized using a mortar and a pestle. The homogenized ash and soil samples were sieved using a 10-mesh 2 mm pore size nylon sieve (Zhangxing Instrument, Hangzhou, Zhejiang, China) to remove large particles. The sieved samples were stored in 15 mL acid-washed centrifuge tubes in a −20 °C freezer. They were also sorted into classes based on their color based on visual inspection (Fig. S4).

3.3. Electron paramagnetic resonance

The EPR spectra in the WUI fire ash and soil samples were recorded at room temperature using an X-band Bruker EMX electron paramagnetic resonance spectrometer (Bruker Corporation, Billerica, Massachusetts, United States), operating in the high frequency (100 kHz) magnetic field modulation mode and a microwave frequency of 9.38 GHz. The EPR analyses were performed approximately 12 months after sample collection. A first set of experiments (all ash samples) was performed to detect organic free radicals (*g*-value = 2.003–2.005) using a narrow magnetic field range with the following experimental conditions: sweep width 200 Gauss (G), sweep time 30 s, modulation amplitude 2.00 G, central field 3350 G, and microwave power 1.59 mW. A second set of experiments (LNU Lightning Complex Fire ashes only) was performed to detect transition metal spins (*e.g.,* g-values of 2.0–1.7 for Mn^{2+}, 2.2–2.0 for Cu^{2+}, and 4.3–2.2 for Fe^{2+}, depending on coordination environment, ligand field strength, and presence of neighboring paramagnetic centers) using a wider magnetic field range with the following experimental conditions: sweep width 5500 G, sweep time 275 s, modulation amplitude 2 G, central field 3350 G, and microwave power 1.59 mW. The LNU Lightning Complex Fire ash samples samples were selected for the broader EPR scans because many (14 out of 31) of these ash samples displayed transition metal spin peaks whereas only few (3 out of 22) NC Fire ash displayed transition metal spin peaks. Measurements were performed using cylindrical EPR quartz tubes (4 mm × 250 mm) and a sample weight of approximately 50 mg. The concentration of environmentally persistent organic free radicals (centered around g = 2.003–2.005) were calculated using TEMPO (2,2,6,6,-tetramethylpiperedine-*l*-oxyl; molecular weight 156.25 g/mol) as a standard due to similarity of the spectral profiles of TEMPO and EPFRs (Abdel-Rahman et al., 2016; Zaunschirm et al., 2018). Briefly, the EPR signal was calibrated using free radical trap standard TEMPO prepared at different concentrations in benzene (0, 5×10^{-7}, 5×10^{-6}, 8×10^{-6}, 2×10^{-5}, 5×10^{-5}, 7.5×10^{-5}, 1×10^{-4}, 1.5×10^{-4}, and 5×10^{-4} mol/L). The area under the first derivative of the organic radical absorption spectrum in the ash samples and the free radical trap standard TEMPO was determined by double integration. The concentration of radicals was determined using the following equation -

$$y = m\,X \frac{Volume\ of\ trap\ (L)}{Mass\ of\ ash\ sample\ (g)}$$

where, y = free radical concentration (spins per gram (g^{-1})), m = slope of the calibration curve, e.g., concentration of free radicals in TEMPO (spins L^{-1}) *vs.* the TEMPO double integrated area of the first derivative of the organic radical absorption spectrum, X = double integrated area of the first derivative of the organic radical absorption spectrum for the ash samples, and volume of trap = 100 μL.

The concentration of transition metal spins was not determined in this study because it was not possible to accurately double integrate the EPR spectra. Transition metal complexes often have broad EPR lines due to large zero-field splitting and g-anisotropy and the presence of multiple transition metal oxidation and spin states which result in overlapped EPR signals (Petasis and Hendrich, 2015). The effective *g*-value (g_{eff}) was determined using the following equation:

$$g = \frac{\hbar\nu}{\beta H_0}$$

where g is a constant of proportionality, whose value is the property of the electron in a certain environment, ħ is Plank's constant, ν is the microwave frequency, β is the Bohr magneton, and B is H_0 is the magnetic field resonance. The hyperfine splitting constant A was calculated as the arithmetic mean of the difference of the resonance field values of neighboring lines.

4. Results and discussion

4.1. EPR spectra features

Previous studies on EPFRs in environmental samples such as particulate matter (Saravia et al., 2013; Wang et al., 2018), biochar (Huang et al., 2020; Odinga et al., 2020; Ruan et al., 2019), hydrothermal carbonization of sewage sludge (Zhu et al., 2019), and wildfire charcoal (Sigmund et al., 2021) using EPR typically focused on a narrow magnetic field range (*e.g.,* 3250 to 3450 G) and reported EPR signals typical of carbon- and/or oxygen-centered radicals, similar to those shown in Fig. S5a, with an effective g-value of 2.003–2.005, respectively (Sigmund et al., 2021). Initially, we followed the same strategy and detected EPR signals with a magnetic field at resonance (H_0) of 3344 G, resonance line width (ΔH_{pp}) of 5 G, and an effective g-value of 2.005, typical of the oxygen-centered radicals. Oxygen-centered EPFRs are stable in air, whereas carbon-centered EPFRs are not (Odinga et al., 2020), which may explain why only oxygen-centered EPFRs were detected in all ash samples in this study. It is possible that carbon-centered EPFRs indirectly

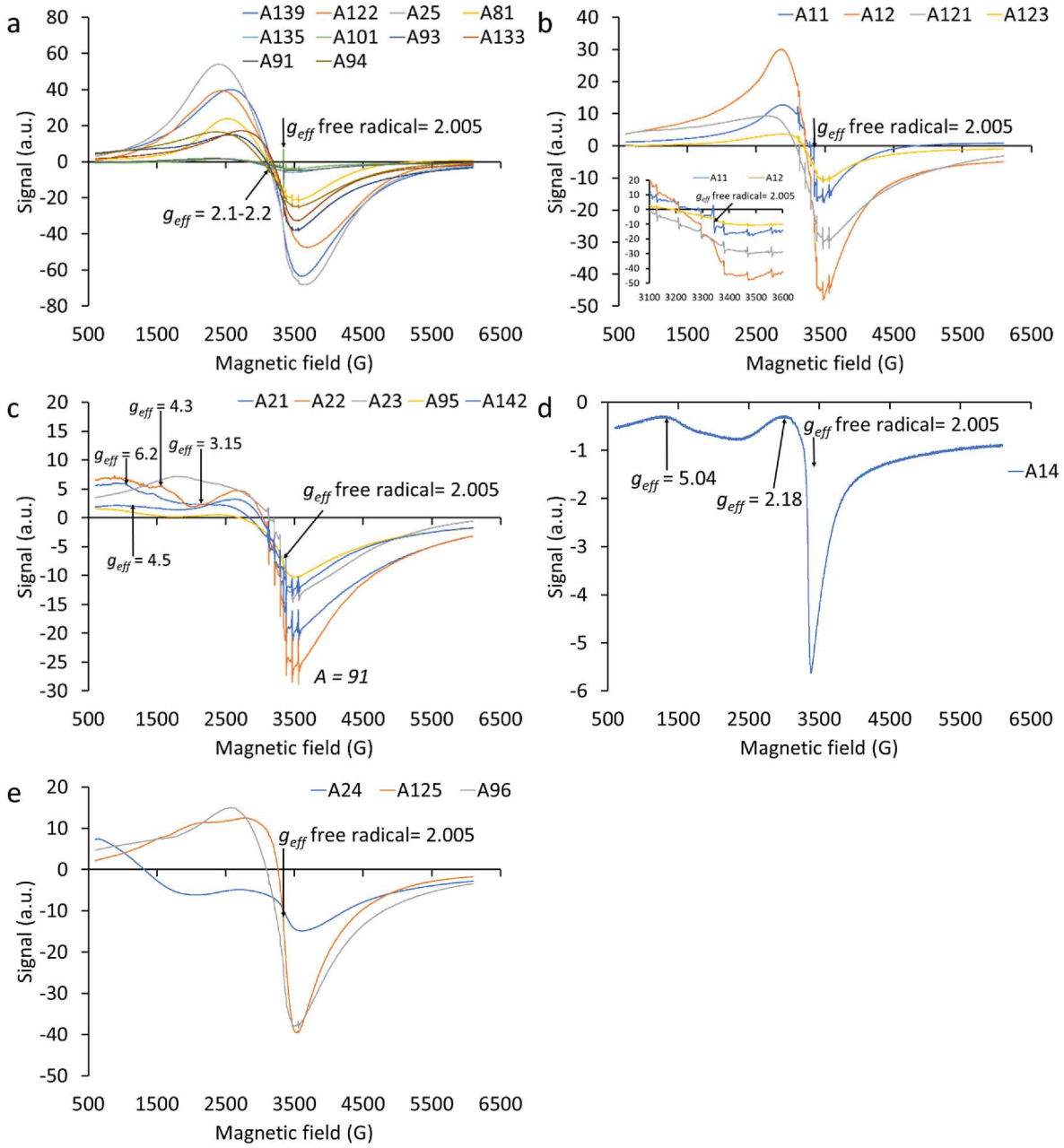

Fig. 1. Typical electron paramagnetic resonance signals (in arbitrary units (a.u.)) observed in fire ashes when scanning a wide magnetic field (500–6500 G). All spectra display broad signals ascribed to different types of nanoparticles overlapped with other signals, including: (a) oxygen-centered environmentally persistent free radicals, (b) six-line hyperfine structures typical of Mn^{2+}, (c) six-line hyperfine structures typical of Mn^{2+} together with other transition metal peaks (d) spectrum of likely Cu^{2+} species with effective g-values (g_{eff}) of 2.18, and 5.04, and (e) spectra of likely chromated copper arsenate related nanomaterials. Ash samples are described in Table S1.

formed oxygen-centered EPFRs during their degradation. However, we also observed the presence of peaks other than those typical of oxygen-centered radicals (Fig. S5b). These peaks are indicative of the presence of paramagnetic species other than EPFRs in the WUI fire ash, which have not been previously explored by EPR in WUI fire ash. Most likely these non-EPFR signals are due to transition metals which tend to exhibit transitions over a fairly broad field range. It is worth noting that all ash samples contain high concentrations of transition metals such as Co, Cr, Cu, Fe, Mn, Ni, and titanium (Ti) which occur in the form of nanomaterials (Alam et al., 2023; Alshehri et al., 2023; Baalousha et al., 2022). Identified nanomaterial phases in the studied fire ash include, among others, maghemite (ϒ-Fe_2O_3), magnetite (Fe_3O_4), wüstite (FeO), and zero valent iron (Baalousha et al., 2022); chromated copper arsenate related nanomaterials ($CuCrO_2$, $CuCr_2O_4$) (Alam et al., 2023); anatase (TiO_2), rutile (TiO_2), and Magnéli titania (Ti_nO_{2n-1}) Mn-bearing nanomaterials such as manganite (γ-$Mn^{3+}OOH$), hausmannite ($Mn^{2+}Mn_2^{3+}O_4$), rhodochrosite ($Mn^{4+}CO_3$), and Mn_2O_3 (tentative identification of the phases) CuSn and CuPb alloys; SnPb, SbPb, and SnSb alloys; CoAl alloys; and zincite). Several of these nanomaterials and metal oxidation states can result in EPR signals as discussed below.

4.2. Non-EPFR paramagnetic species in wildland-urban interface ashes

To further identify the paramagnetic species leading to the additional EPR signals in the fire ash, we scanned a wider magnetic field range (*e.g.,* 600 to 6100 G). The EPR spectra recorded in the different ash samples showed broad peaks (Fig. 1). Similar EPR signals were obtained for paramagnetic metal-bearing particles such as maghemite (Guskos et al., 2002; Sibera et al., 2009), magnetite (Fe_3O_4) (Guskos et al., 2002), hematite (α-Fe_2O_3) (Guskos et al., 2002), and MnO_2 (Guskos et al., 2002; Kakazey et al., 2001; Stegarescu et al., 2020). The broadness of the EPR resonance signal can be ascribed to dipole-dipole and exchange interactions between the paramagnetic ions (Kakazey et al., 2001) and the random orientation of the paramagnetic species, which scatter in directions of the anisotropic field of the particles (Shahane et al., 2013). The magnetic field at resonance (H_0), resonance line width (ΔH_{pp}), and the effective *g*-value (g_{eff}) for the broad peaks are summarized in Table S2, which cover a wide range of effective *g*-values. The high magnitude of the line width and *g*-values can be attributed to the magnetic dipole interactions among particles and the super exchange interaction between the magnetic ion and the oxygen ion (Li et al., 2000). Below we discuss in detail the various potential paramagnetic species in the fire ashes in light of the EPR signals and nanomaterials identified in the fire ashes in our previous studies (Alam et al., 2023; Alshehri et al., 2023; Baalousha et al., 2022).

The EPR spectra of some ash displayed a first derivative of a broad Gaussian peak (Fig. 1a). The effective *g*-values were typical of magnetic iron oxide nanoparticles (*e.g.,* 2.08–2.33 for α-Fe_2O_3, ϒ-Fe_2O_3, and Fe_3O_4) (Guskos et al., 2002; Lee et al., 2011; Wang et al., 2013). These observations are consistent with our previous studies which demonstrated a relatively high concentration of iron in all ashes and that magnetic iron oxide nanoparticles (*e.g.,* magnetite and maghemite) were the dominant type of iron oxide nanoparticles in the ashes accounting for 2–100% of iron with a median value of 63% (Alshehri et al., 2023; Baalousha et al., 2022). The variability in the effective *g*-value can be ascribed to the coordination environment, ligand field strength, and presence of neighboring paramagnetic centers.

Some ash samples displayed EPR spectra indicating the presence of aggregated Mn ions inside a crystal lattice or on the surface of particles, as well as isolated Mn^{2+} within the lattice of other types of particles. EPR spectra consisted of the first derivative of a broad Gaussian peak with an effective *g*-value of 2.005 (Fig. 1b) overlapped with six-line hyperfine structures with an isotropic hyperfine splitting constant $A = 91$ to 98 G centered at $g_{eff} = 2.005$. Other ash samples displayed EPR spectra with a first derivative of a non-Gaussian broad peak superimposed with six-line hyperfine structures with an isotropic hyperfine splitting constant $A =$ 91 G centered at $g_{eff} = 2.005$ (Fig. 1c). In addition, these ash samples displayed small well-defined peaks at high g_{eff}-values (*e.g.,* 3.15, 4.3, 4.5, and 6.2) (Fig. 1c). Aggregated Mn ions in nanoparticles are characterized by a single exchange-narrowed line with a signal width of 600 G, which indicates that the broad signal might be attributed to dipole-dipole interactions between Mn ions (Galyametdinov et al., 2019; Kakazey et al., 2001; Stegarescu et al., 2020). Isolated Mn^{2+} ions in crystal lattice of nanoparticles (*e.g.,* Mn^{2+} in calcite) generate well distinguishable six-component signals with the hyperfine splitting constant A = 94 G (Garribba and Micera, 2006; Kim et al., 2011). Divalent manganese in a crystalline field of cubic symmetry has a paramagnetic resonance spectrum with six lines originating from the interaction between the Mn^{2+} electron cloud and the ^{55}Mn nucleus of spin I = 5/2. Therefore, the broad signal in the EPR spectra in Fig. 1b and c indicates that Mn ions form aggregates (*e.g.,* clusters/nanoparticles) inside a crystal lattice and on the surface of particles, while the six-line hyperfine structures indicate that Mn ions occurred as isolated Mn^{2+} inside the lattice of other types of particles (Garribba and Micera, 2006; Kim et al., 2011). Additionally, the effective *g*-value = 2.005 is consistent with that of MnO_2 particles (Kakazey et al., 2001; Stegarescu et al., 2020). The variation in the hyperfine splitting constant (A) can be ascribed to the presence of different Mn^{2+} sites or to the variation of the Mn^{2+} atomic environment in the different ash samples (Ledoux et al., 2002; Nistor et al., 2010). Previous studies demonstrated that the average splitting of these six lines decreases with covalent bonding and exchange interactions with Mn^{2+} neighbors (Van Wieringen, 1955). The signal at $g_{eff} = 4.3$ could be ascribed to isolated Fe^{3+} ions (Fig. 1c) (Ledoux et al., 2002). The signal at low magnetic field (Fig. 1c) can be ascribed to ferromagnetic phases containing Mn (Ledoux et al., 2002). It is worth noting that EPR analysis is insufficient to determine the exact phase of the Mn^{2+} or its surrounding atomic environment. The phase determination of Mn^{2+}-bearing particles will be performed using x-ray absorption spectroscopy in future studies as performed for iron in our previous study (Baalousha et al., 2022). Furthermore, whereas some EPR spectra displayed a signal typical of oxygen-centered free radical, other EPR spectra lacked the oxygen-centered free radical signal, which may be in part a consequence of the radical spin quenching effect of metal complexation as found for humic substances (Jerzykiewicz et al., 2002).

The EPR spectrum of ash sample A14 displayed a narrow asymmetrical peak typical of Cu^{2+} complexes (Fig. 1d) (Pacioni et al., 2013). Ash A14 is composed chiefly of Ti, Mn, Fe, Ni, Cu, Zn, Sb, Ba, and Pb (Alshehri et al., 2023). The EPR spectra in Fig. 1e are complex and most likely result from a combination of multiple paramagnetic species including Fe-, Cr-, and Cu-oxide particles, which can be attributed to chromated copper arsenate nanoparticles (Humar et al., 2004; Mazela et al., 2005). The EPR signal in Fig. 1e is attributed to chromated copper arsenate nanoparticles because samples A24 and A125, and to a lesser extent A96 are composed mainly of chromium, copper, and arsenic (Alam et al., 2023). High resolution-transmission electron microscopy analysis coupled with electron diffraction revealed that these ashes contain various types of nanoparticles including CrO_3, CrO_2, Cr_2O_3, $CuCrO_2$, $CuCr_2O_4$, $CrAsO_4$, $Cr_2As_4O_{12}$, As_2O5, AsO_2, As_2O_3, and As_4O_6 (Alam et al., 2023). The main paramagnetic species in these phases are Cr^{3+} or Cu^{2+}. The species Cr^{6+}, Cr^{4+}, and Cu^{1+} are nonparamagnetic, so they are EPR-silent species (Puzon et al., 2005).

Fig. 2a displays the correlation between the double-integrated area under the broad peak and the concentration of magnetic (magnetite and maghemite) particles in the fire ashes (Baalousha et al., 2022). A moderate correlation was observed between the area of the peak and the concentration of magnetic particles in the ashes, suggesting that the broad EPR peaks can be partially attributed to the presence of magnetic nanoparticles in the fire ash. Fig. 2b displays the correlation between the double-integrated area under the broad peak and the concentration of Cu and Cr in the three ashes that predominantly contained chromated copper arsenate residues (Alam et al., 2023). Negative correlations were observed between the area of the peak and the concentration of Cu and

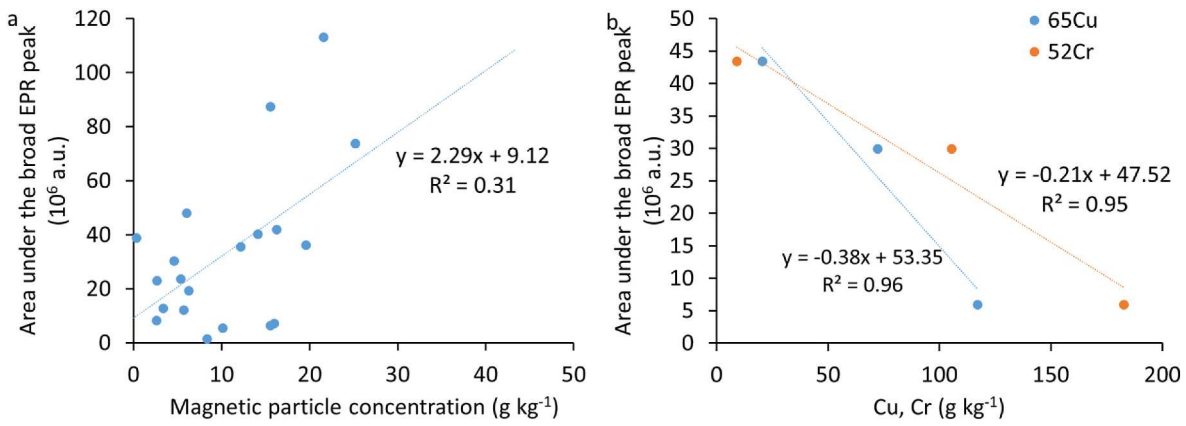

Fig. 2. Correlation between the integrated area under the broad peak and the concentration of (a) magnetic particle (magnetite and maghemite) concentration in grams per kilogram (g kg^{-1}), and (b) copper (Cu) and chromium (Cr) in fire ashes. The concentration of magnetic particles were taken from (Baalousha et al., 2022).

Cr. Overall, these findings are in good agreement with the elemental composition and iron solid phase speciation of the various ash samples (Alshehri et al., 2023; Baalousha et al., 2022).

4.3. Impact of ash source and color on EPFR concentrations

Forty-five of the analyzed fifty-three soil and ash samples contained EPFR concentrations ranging from 2.12×10^{14} to 3.04×10^{17} spin g^{-1} (Fig. 3a). These EPFR concentrations are of the same order of magnitude as those reported for soils and airborne particulate matter (10^{16} to 10^{17} spins g^{-1}, Table S3) (Vejerano et al., 2018), but are an order of magnitude lower than those reported in wildfire ash (10^{18} to 10^{19} spins g^{-1}) (Sigmund et al., 2021), and biochar (10^{18} to 10^{19} spins g^{-1}) (Odinga et al., 2020). The lower EPFR concentrations in wildland-urban interface fire ash measured in this study compared to those reported in wildfire ash by Sigmund et al. (2021) can be attributed to differences in the ash source, carbon content, or time of EPFR measurement after fuel combustion. The carbon content in the ash reported in Sigmund et al. (2021) (*e.g.,* 58–90 %) were higher than those reported in this study (0.6–47.6%, Fig. S6) (Alshehri et al., 2023). Additionally, the EPFR measurement in this study was performed approximately one year after the fire occurred which may have resulted in a decrease in EPFR concentrations.

The EPFRs were detected in all soil and vegetation ash samples, in twenty-four out of thirty structural ash samples, and in two out of the four vehicle ash samples (Table S4). The mean EPFR concentrations in ash decreased following the order vegetation ash ($1.1 \times 10^{17} \pm 1.1 \times 10^{17}$ spins g^{-1}) > structural ash ($1.6 \times 10^{16} \pm 3.7 \times 10^{16}$ spins g^{-1}) > vehicle ash ($6.4 \times 10^{15} \pm 8.6 \times 10^{15}$ spins g^{-1}) > soil ($3.2 \times 10^{15} \pm 3.7 \times 10^{15}$ spins g^{-1}, Table S4). This order is generally consistent with the increase of carbon content in these types of fuel (*i.e.,* soil < structure < vegetation, with the exception of vehicle ash which has the highest carbon content due to the use of plastics in various vehicle components, Fig. S6b). Other controls that could determine EPFR concentrations in ash include the temperature each fuel experienced during the fire and the likelihood of combustion completeness. Although vegetation and structures may experience temperatures up to >1000 °C during fires, the soil surface temperature could reach a maximum of 850 °C during wildfires and decreases to <400 °C at 1 cm below the surface (Certini, 2005; DeBano, 2000; DeBano et al., 1979, 1998; Li et al., 2012). Thus, the low heating temperature (*e.g.,* insufficient for organic matter pyrolysis) of soil organic matter may lead to lower EPFR concentrations compared to those in vegetation and structures which experience higher temperatures, which may lead to higher degree of carbonization. Structural wood contains less water than living vegetation and is therefore more likely to experience a more complete combustion during fire and thus consumption of organic matter, explaining the lower EPFR concentrations in structural ashes than vegetation ashes. Additionally, the higher lignin content of vegetation also leads to less complete combustion during fires (Alshehri et al., 2023), which would promote EPFRs formation. The high carbon content in vehicle ash is attributed to the use of the thermally stable black-carbon additives in vehicle parts, including tires and automobile interiors such as ventilation flaps, radiators, and airbags (Koreňová et al., 2006). The thermal stability of black carbon may limit the formation of EPFRs during combustion processes.

The mean EPFR concentrations were highest in black ashes and

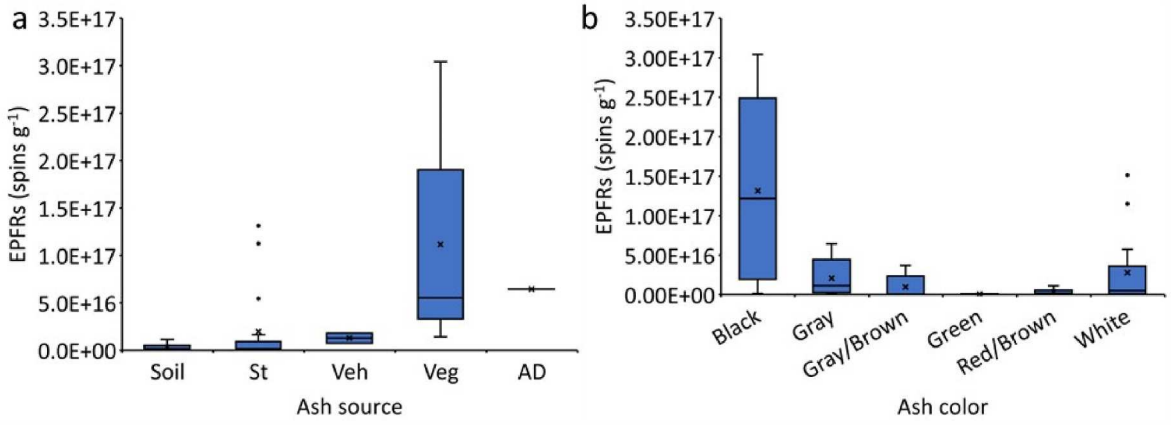

Fig. 3. Concentration of environmentally persistent free radicals (EPFRs) as a function of (a) ash source and (b) ash color. St: structure, Veh: vehicle, Veg: vegetation, and AD: atmospheric deposition.

decreased following the order black ($1.1 \times 10^{17} \pm 1.1 \times 10^{17}$ spins g^{-1}) > white ($2.5 \times 10^{16} \pm 4.4 \times 10^{16}$ spins g^{-1}) > gray ($1.8 \times 10^{16} \pm 2.4 \times 10^{16}$ spins g^{-1}) > gray/brown ($6.9 \times 10^{15} \pm 1.4 \times 10^{16}$ spins g^{-1}) > red/brown ($3.5 \times 10^{15} \pm 3.9 \times 10^{15}$ spins g^{-1}) > green ($3.9 \times 10^{14} \pm 5.1 \times 10^{14}$ spins g^{-1}, Fig. 3b and Table S5). This suggests that EPFR concentrations decrease with increased combustion completeness. This is consistent with the increase in EPFR concentrations in wildfire ashes with the carbonization degree (*e.g.,* increase in carbon content and decrease in oxygen/carbon (O/C) molar ratio), which depends on the properties of the fire fuel and the fire conditions such as temperature, duration, and oxygen availability (Sigmund et al., 2021). EPFRs form during thermal processes through the decomposition of organic precursors such as phenols, halogenated phenols, and quinone-type molecules (Liu et al., 2021). The increased combustion temperature facilitates the decomposition of phenolic compounds, and thus EPFRs, in biomass leading to decreased EPFR concentration with increased combustion completeness.

4.4. Effect of ash source and color on manganese speciation

Detailed examination of the six-line hyperfine EPR signal (Fig. 4a) revealed six primary, intense lines due to allowed transitions ($\Delta m = \pm 0$) with a hyperfine splitting constant of 91 G (ash samples A21, A22, A23, A94, and A142) and 98 G (A101) and g_{eff} of 2.005 and 10 secondary lines with intensities much weaker than primary lines due to forbidden transition ($\Delta m = \pm 1$). The hyperfine splitting is related to electron-nuclear interactions and molecular structure. These EPR spectra are attributed to the presence of reduced Mn^{2+} species as discussed above in section 3.2.

Reduced manganese (Mn^{2+}) ions were observed mainly in fire ashes with higher combustion completeness (*e.g.,* gray and white ash, Fig. 4b) and were not observed in black or green ashes. The relative amounts of Mn^{2+} ions were determined by double integrating the area under one of the six lines (proxy for Mn^{2+} ion concentration, $g_{eff} = 1.98$). The relative amounts of Mn^{2+} ions (double-integrated peak area) was highest in structural gray ash (median = 8109 arbitrary units (a.u.), n = 3), structural white ash (median = 5347 a.u., n = 9), and vegetation gray ash (5373 a.u., n = 2, Fig. 4b), indicating a trend of increased Mn^{2+} ions reduction as combustion completion increased by reducing agents released by the combustion process such as H_2, CH_4, C, and CO. Manganese is commonly found in natural environments as Mn^{2+}, Mn^{3+}, and Mn^{4+}; Mn^{2+} is favored under reducing conditions such as those that occur in the fire environment. All reduction reactions are highly endothermic requiring high amounts of thermal energy (Goel, 1994). For instance, the transition temperatures of MnO_2 to Mn_2O_3, Mn_3O_4, and MnO in air are 500, 900, and 1700 °C, respectively (Stobbe et al., 1999), demonstrating that heating alone in the fire environment is insufficient for the reduction of Mn species to Mn^{2+}. However, in the presence of reducing agents such as H_2, CH_4, C, and CO, the reduction of manganese oxides occurs at lower temperatures, suggesting that the release of reducing agents during combustion processes drives the reduction of Mn species to Mn^{2+}. For instance, manganese oxides can be reduced to MnO_2 with methane at 450 °C (Stobbe et al., 1999) and with hydrogen this reduction can occur between 275 and 400 °C, depending on the hydrogen partial pressure (De Bruijn et al., 1980). In this study, reduced manganese species were formed in wildland-urban fire hotspots, where higher combustion completeness was achieved, as evidenced by the presence of gray and white ashes.

5. Environmental and human health implications

This study demonstrated that fire ash represents a substantial source of paramagnetic species such as EPFRs, transition metals, and transition metal oxide clusters/particles (*e.g.,* Fe^{3+}, Mn^{2+} and Cu^{2+}) into the environment. Fire ashes, and thus the identified paramagnetic species, are highly mobile during and following WUI fires, can be transported by wind or water following precipitation, and eventually reach hydrological networks (Coppola et al., 2018; Jones et al., 2020). Wind transport of fire ash occurs on a global scale and exposes large populations to ash-associated contaminants. Post-fire transport of fire ash with runoff following precipitation mobilizes the deposited fire ash to surface waters. When in contact with surface water (*e.g.,* in the atmosphere, rivers, lakes, or oceans), pore water in soils, or biological fluids (*e.g.,* lung fluids), EPFRs react with hydrogen peroxide forming various types of reactive oxygen species (ROS) - such as the hydroxyl radical, superoxide, or singlet oxygen (Khachatryan et al., 2011; Pignatello et al., 2017; Tong et al., 2017). These reactive free radicals may cause oxidative stress in aquatic organisms and humans (Lushchak, 2011). Even at low concentrations, EPFRs-derived ROS in environmental systems influence ecosystem functions in many ways, including among others, transformation of natural organic matter (Waggoner et al., 2017), plant seed germination (Liao et al., 2014), and enzymatic activity (Liu et al., 2018), and may have adverse effects on algae (Zhang et al., 2019b), bacteria (Zhang et al., 2019a) and invertebrates (Lieke et al., 2018). The health risks arising from EPFRs in fine atmospheric particulate matter ($PM_{2.5}$) have been shown to be similar to those of cigarette smoking and could explain why some non-smokers develop cancers similar to those seen in smokers (Dellinger, 2008; Pryor et al., 1983). EPFRs have also been shown to cause DNA damage (Khachatryan et al., 2011).

The environmental implications of paramagnetic iron oxide nanoparticles such as maghemite and magnetite are discussed elsewhere (Baalousha et al., 2022). Briefly, magnetic iron oxide nanoparticles have

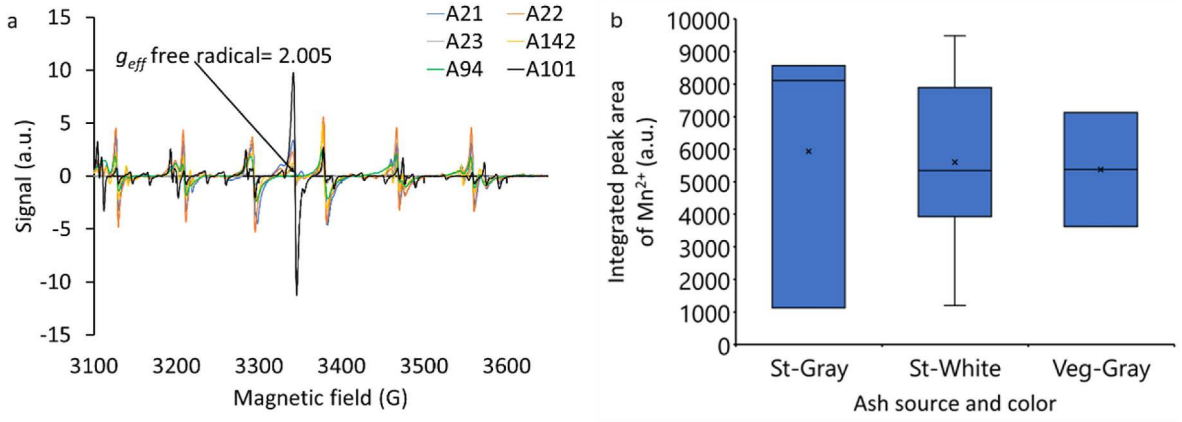

Fig. 4. (a) Typical electron paramagnetic resonance signals (in arbitrary units (a.u.)) observed in fire ashes focusing on the Mn^{2+} signal, and (b) integrated peak area of Mn^{2+} as a function of ash source and color. St and Veg refer to structural and vegetation ash.

been linked to neurodegenerative disease (Hautot et al., 2003; Pankhurst et al., 2008) and global warming (Matsui et al., 2018). Manganese oxides play an important role in controlling biogeochemical element cycling (Owings, 2020). Manganese oxides are considered to be the strongest, naturally occurring oxidant and are capable of transforming a wide range of organic substrates (Remucal and Ginder-Vogel, 2014). Manganese oxide nanoparticles have been shown to be neurotoxic (Máté et al., 2016) and possess pro- and anti-oxidant activities, including oxidase-, catalase-, and superoxide dismutase-like activities (Jiang et al., 2020).

The environmental and human health implications of WUI fires are projected to increase in the future because fire frequency and severity are increasing worldwide due to human activities and climate change (Goss et al., 2020; Minott, 2017; Williams et al., 2019). For instance, the annual burned area in California has increased by over 500% over the past five decades (Williams et al., 2019). Ecosystems that used to be less prone to wildfires, such as tropical rainforests or arctic tundra, are now the sites of extensive fires (Bowman et al., 2020; Silva et al., 2018). Wildfires are also spreading to the WUI due to the increasing human population in this land-use type, with an estimated 2.0 million housing units in California and 6.9 million housing units in the United States located in areas identified as having a high risk of burning in a wildfire event (Minott, 2017). Fires at the wildland-urban interface consume fuels rich in metals and metallic nanoparticles used in structural materials such as pigments and wood preservatives, releasing paramagnetic species other than EPFRs into the natural environment. These potential environmental and health effects of WUI fires justify further investigation.

CRediT authorship contribution statement

Mahbub Alam: Writing – review & editing, Writing – original draft, Formal analysis, Data curation. **James D. Sitter:** Writing – review & editing, Formal analysis. **Aaron K. Vannucci:** Writing – review & editing. **Jackson P. Webster:** Writing – review & editing. **Sandrine J. Matiasek:** Writing – review & editing. **Charles N. Alpers:** Writing – review & editing. **Mohammed Baalousha:** Writing – review & editing, Supervision, Methodology, Investigation, Data curation, Conceptualization.

Declaration of competing interest

The authors declare that they have no known competing financial interests or personal relationships that could have appeared to influence the work reported in this paper.

Data availability

Data will be made available on request.

Acknowledgments

This work was supported by a RAPID grant (2101983) from the U.S. National Science Foundation (NSF), and by the U.S. Geological Survey through the Environmental Health Program of the Ecosystem Mission Area. We would like to thank Dr. Peggy O'Day for comments on the manuscript before submission. Any use of trade, firm, or product names is for descriptive purposes only and does not imply endorsement by the U.S. Government.

Appendix A. Supplementary data

Supplementary data to this article can be found online at https://doi.org/10.1016/j.chemosphere.2024.142950.

References

Abdel-Rahman E, A., Mahmoud, A.M., Khalifa, A.M., Ali, S.S., 2016. Physiological and pathophysiological reactive oxygen species as probed by EPR spectroscopy: the underutilized research window on muscle ageing. The Journal of physiology 594, 4591–4613.

Alam, M., Alshehri, T., Wang, J., Singerling, S.A., Alpers, C.N., Baalousha, M., 2023. Identification and quantification of Cr, Cu, and as incidental nanomaterials derived from CCA-treated wood in wildland-urban interface fire ashes. J. Hazard Mater. 445, 130608.

Alshehri, T., Wang, J., Singerling, S.A., Gigault, J., Webster, J.P., Matiasek, S.J., et al., 2023. Wildland-urban interface fire ashes as a major source of incidental nanomaterials. J. Hazard Mater. 443, 130311.

Ayscough, P.B., 1967. Electron Spin Resonance in Chemistry. Methuen, London, p. 451.

Baalousha, M., Desmau, M., Singerling, S., Webster, J.P., Matiasek, S., Stern, M.A., et al., 2022. Discovery and potential ramifications of reduced iron-bearing nanomaterials—magnetite, wüstite, and zero valent iron—in wildland-urban interface fire ashes. Environ. Sci.: Nano 9, 4149.

Berliner, L.J., Reuben, J., 2012. Spin Labeling: Theory and Applications, 8. Springer Science & Business Media.

Bodí, M.B., Martin, D.A., Balfour, V.N., Santín, C., Doerr, S.H., Pereira, P., et al., 2014. Wildland fire ash: production, composition and eco-hydro-geomorphic effects. Earth Sci. Rev. 130, 103–127.

Bowman, D.M., Kolden, C.A., Abatzoglou, J.T., Johnston, F.H., van der Werf, G.R., Flannigan, M., 2020. Vegetation fires in the anthropocene. Nat. Rev. Earth Environ. 1, 500–515.

Burton, C.A., Hoefen, T.M., Plumlee, G.S., Baumberger, K.L., Backlin, A.R., Gallegos, E., et al., 2016. Trace elements in stormflow, ash, and burned soil following the 2009 station fire in Southern California. PLoS One 11, e0153372.

CALFire, 2022. LNU lightning complex (includes hennessey, gamble, 15-10, Spanish, markley, 13-4, 11-16, walbridge) incident. https://www.fire.ca.gov/incidents/2020/8/17/lnu-lightning-complex-includes-hennessey-gamble-15-10-spanish-markley-13-4-11-16-walbridge/.

Campos, I., Abrantes, N., Keizer, J.J., Vale, C., Pereira, P., 2016. Major and trace elements in soils and ashes of eucalypt and pine forest plantations in Portugal following a wildfire. Sci. Total Environ. 572, 1363–1376.

Certini, G., 2005. Effects of fire on properties of forest soils: a review. Oecologia 143, 1–10.

Coppola, A.I., Wiedemeier, D.B., Galy, V., Haghipour, N., Hanke, U.M., Nascimento, G.S., et al., 2018. Global-scale evidence for the refractory nature of riverine black carbon. Nat. Geosci. 11, 584–588.

De Bruijn, T.J.W., Soerawidjaja, T.H., De Jongt, W.A., Van Den Berg, P.J., 1980. Modelling of the reduction of manganese oxides with hydrogen. Chem. Eng. Sci. 35, 1591–1599.

DeBano, L.F., 2000. The role of fire and soil heating on water repellency in wildland environments: a review. J. Hydrol. 231, 195–206.

DeBano, L.F., Neary, D.G., Ffolliott, P.F., 1998. Fire Effects on Ecosystems. John Wiley & Sons.

DeBano, L.F., Rice, R.M., Eugene, C.C., 1979. Soil heating in chaparral fires: effects on soil properties, plant nutrients, erosion, and runoff. In: Res. Paper PSW-RP-145, 21. US Department of Agriculture, Forest Service, Pacific Southwest Forest and Range Experiment Station, Berkeley, CA, p. 145.

Dellinger, B., 2008. Newly Detected Air Pollutant Mimics Damaging Effects of Cigarette Smoke. American Chemical Society 236th National Meeting, Philadelphia, PA, USA. August, pp. 17–21.

Galyametdinov, Y.G., Sagdeev, D.O., Sukhanov, A.A., Voronkova, V.K., Shamilov, R.R., 2019. Monitoring of the mechanism of Mn ions incorporation into quantum dots by optical and EPR spectroscopy. In: Photonics, 6. Multidisciplinary Digital Publishing Institute, p. 107.

Garribba, E., Micera, G., 2006. Determination of the hyperfine coupling constant and zero-field splitting in the ESR spectrum of Mn2+ in calcite. Magn. Reson. Chem. 44, 11–19.

Goel, R., 1994. Thermodynamic Considerations in the Production of Bulk Ferro Alloys (Fe-Mn, Fe-Cr and Fe-Si.

Goss, M., Swain, D.L., Abatzoglou, J.T., Sarhadi, A., Kolden, C.A., Williams, A.P., et al., 2020. Climate change is increasing the likelihood of extreme autumn wildfire conditions across California. Environ. Res. Lett. 15, 094016.

Guskos, N., Papadopoulos, G.J., Likodimos, V., Patapis, S., Yarmis, D., Przepiera, A., et al., 2002. Photoacoustic, EPR and electrical conductivity investigations of three synthetic mineral pigments: hematite, goethite and magnetite. Mater. Res. Bull. 37, 1051–1061.

Hautot, D., Pankhurst, Q.A., Khan, N., Dobson, J., 2003. Preliminary evaluation of nanoscale biogenic magnetite in Alzheimer's disease brain tissue. Proc. Roy. Soc. Lond. B Biol. Sci. 270, S62–S64.

Huang, Y., Guo, X., Ding, Z., Chen, Y., Hu, X., 2020. Environmentally persistent free radicals in biochar derived from Laminaria japonica grown in different habitats. J. Anal. Appl. Pyrol. 151, 104941.

Humar, M., Pohleven, F., Šentjurc, M., 2004. Effect of oxalic, acetic acid, and ammonia on leaching of Cr and Cu from preserved wood. Wood Sci. Technol. 37, 463–473.

Inciweb. Incident information system. North Complex https://inciweb.nwcg.gov/incident/6997/2022.

Ivarsson M, Broman C, Gustafsson H, Holm NG. Biogenic Mn-oxides in subseafloor basalts. PLoS One 2015; 10: e0128863.

Jerzykiewicz, M., Jezierski, A., Czechowski, F., Drozd, J., 2002. Influence of metal ions binding on free radical concentration in humic acids. A quantitative electron paramagnetic resonance study. Org. Geochem. 33, 265–268.

Jia, H., Zhao, S., Nulaji, G., Tao, K., Wang, F., Sharma, V.K., et al., 2017. Environmentally persistent free radicals in soils of past coking sites: distribution and stabilization. Environ. Sci. Technol. 51, 6000–6008.
Jiang, X., Gray, P., Patel, M., Zheng, J., Yin, J.-J., 2020. Crossover between anti- and pro-oxidant activities of different manganese oxide nanoparticles and their biological implications. J. Mater. Chem. B 8, 1191–1201.
Johnston, S.G., Bennett, W.W., Burton, E.D., Hockmann, K., Dawson, N., Karimian, N., 2018. Rapid arsenic(V)-reduction by fire in schwertmannite-rich soil enhances arsenic mobilisation. Geochem. Cosmochim. Acta 227, 1–18.
Johnston, S.G., Karimian, N., Burton, E.D., 2019. Fire promotes arsenic mobilization and rapid arsenic (III) formation in soil via thermal alteration of arsenic-bearing iron oxides. Front. Earth Sci. 7, 139.
Jones, M.W., Coppola, A.I., Santín, C., Dittmar, T., Jaffé, R., Doerr, S.H., et al., 2020. Fires prime terrestrial organic carbon for riverine export to the global oceans. Nat. Commun. 11, 2791.
Kakazey, M., Ivanova, N., Sokolsky, G., Gonzalez-Rodriguez, J., 2001. Electron paramagnetic resonance of MnO2 powders. Electrochem. Solid State Lett. 4, J1.
Khachatryan, L., Vejerano, E., Lomnicki, S., Dellinger, B., 2011. Environmentally persistent free radicals (EPFRs). 1. Generation of reactive oxygen species in aqueous solutions. Environ. Sci. Technol. 45, 8559–8566.
Kilias, S.P., Ivarsson, M., Chi Fru, E., Rattray, J.E., Gustafsson, H., Naden, J., et al., 2020. Precipitation of Mn oxides in quaternary microbially induced sedimentary structures (MISS), cape vani paleo-hydrothermal vent field, milos, Greece. Minerals 10, 536.
Kim, S.S., Bargar, J.R., Nealson, K.H., Flood, B.E., Kirschvink, J.L., Raub, T.D., et al., 2011. Searching for biosignatures using electron paramagnetic resonance (EPR) analysis of manganese oxides. Astrobiology 11, 775–786.
Koreňová, Z., Juma, M., Annus, J., Markoš, J., Jelemenský, L., 2006. Kinetics of pyrolysis and properties of carbon black from a scrap tire. Chem. Pap. 60, 422–426.
Ledoux, F., Zhilinskaya, E., Bouhsina, S., Courcot, L., Bertho, M.-L., Aboukais, A., et al., 2002. EPR investigations of Mn2+, Fe3+ ions and carbonaceous radicals in atmospheric particulate aerosols during their transport over the eastern coast of the English Channel. Atmos. Environ. 36, 939–947.
Lee, J., Choa, Y., Kim, J., Kim, K.H., 2011. Comparison of the magnetic properties for the surface-modified magnetite nanoparticles. IEEE Trans. Magn. 47, 2874–2877.
Li, L., Ishikawa, Y., Mihara, M., 2012. Effects of burning crop residues on soil quality in Wenshui, Shanxi of China. International Journal of Environmental and Rural Development 30–35.
Li, L., Li, G., Smith, R., Inomata, H., 2000. Microstructural evolution and magnetic properties of NiFe2O4 nanocrystals dispersed in amorphous silica. Chem. Mater. 12, 3705–3714.
Liao, S., Pan, B., Li, H., Zhang, D., Xing, B., 2014. Detecting free radicals in biochars and determining their ability to inhibit the germination and growth of corn, wheat and rice seedlings. Environ. Sci. Technol. 48, 8581–8587.
Lieke, T., Zhang, X., Steinberg, C.E., Pan, B., 2018. Overlooked risks of biochars: persistent free radicals trigger neurotoxicity in Caenorhabditis elegans. Environ. Sci. Technol. 52, 7981–7987.
Liu, X., Yang, L., Liu, G., Zheng, M., 2021. Formation of environmentally persistent free radicals during thermochemical processes and their correlations with unintentional persistent organic pollutants. Environ. Sci. Technol. 55, 6529–6541.
Liu, Y., Dai, Q., Jin, X., Dong, X., Peng, J., Wu, M., et al., 2018. Negative impacts of biochars on urease activity: high pH, heavy metals, polycyclic aromatic hydrocarbons, or free radicals? Environ. Sci. Technol. 52, 12740–12747.
Lushchak, V.I., 2011. Environmentally induced oxidative stress in aquatic animals. Aquat. Toxicol. 101, 13–30.
Mabbs, F.E., Collison, D., 2013. Electron Paramagnetic Resonance of D Transition Metal Compounds. Elsevier.
Máté, Z., Horváth, E., Kozma, G., Simon, T., Kónya, Z., Paulik, E., et al., 2016. Size-dependent toxicity differences of intratracheally instilled manganese oxide nanoparticles: conclusions of a subacute animal experiment. Biol. Trace Elem. Res. 171, 156–166.
Matsui, H., Mahowald, N.M., Moteki, N., Hamilton, D.S., Ohata, S., Yoshida, A., et al., 2018. Anthropogenic combustion iron as a complex climate forcer. Nat. Commun. 9, 1593-1593.
Mazela, B., Polus-Ratajczak, I., Hoffmann, S.K., Goslar, J., 2005. Copper monoethanolamine complexes with quaternary ammonium compounds in wood preservation. Biological testing and EPR study. Wood Res. 50, 1–17.
Miller, J.D., Safford, H., Crimmins, M., Thode, A.E., 2009. Quantitative evidence for increasing forest fire severity in the Sierra Nevada and southern Cascade Mountains, California and Nevada, USA. Ecosystems 12, 16–32.
Minott, O., 2017. Which states have the most homes at risk of flooding and wildfires? https://bipartisanpolicy.org/blog/which-states-risk-flooding-wildfires/.
National Interagency Fire Center.Total Wildland Fires and Acres (1983-2020). https://www.nifc.gov/fire-information/statistics/wildfires.
Nistor, S., Stefan, M., Nistor, L., Goovaerts, E., Van Tendeloo, G., 2010. Incorporation and localization of substitutional Mn 2+ ions in cubic ZnS quantum dots. Phys. Rev. B 81, 035336.
Odinga, E.S., Waigi, M.G., Gudda, F.O., Wang, J., Yang, B., Hu, X., et al., 2020. Occurrence, formation, environmental fate and risks of environmentally persistent free radicals in biochars. Environ. Int. 134, 105172.
Owings, S.M., 2020. Importance of Manganese Oxides in Carbon Remineralization in River-Dominated Continental Margins and the Biogeochemical Cycling of Arsenic. Ph.D. Dissertation. Georgia Institute of Technology.
Pacioni, N.L., Filippenko, V., Presseau, N., Scaiano, J.C., 2013. Oxidation of copper nanoparticles in water: mechanistic insights revealed by oxygen uptake and spectroscopic methods. Dalton Trans. 42, 5832–5838.
Pankhurst, Q., Hautot, D., Khan, N., Dobson, J., 2008. Increased levels of magnetic iron compounds in alzheimer's disease. J. Alzheim. Dis. 13, 49–52.
Parra, J.G., Rivero, V.C., Lopez, T.I., 1996. Forms of Mn in soils affected by a forest fire. Sci. Total Environ. 181, 231–236.
Petasis, D.T., Hendrich, M.P., 2015. Quantitative interpretation of multifrequency multimode EPR spectra of metal containing proteins, enzymes, and biomimetic complexes. Methods Enzymol. 563, 171–208. Elsevier.
Petrakis, L., Fraissard, J., 2012. Magnetic Resonance: Introduction, Advanced Topics and Applications to Fossil Energy, 124. Springer Science & Business Media.
Pignatello, J., Mitch, W.A., Xu, W., 2017. Activity and reactivity of pyrogenic carbonaceous matter toward organic compounds. Environ. Sci. Technol. 51, 8893–8908.
Plumlee, G.S., Morman, S.A., Meeker, G., Hoefen, T.M., Hageman, P.L., Wolf, R.E., 2013. The environmental and medical geochemistry of potentially hazardous materials produced by disasters. Treatise on geochemistry 9, 257–304.
Pryor, W.A., Prier, D.G., Church, D.F., 1983. Electron-spin resonance study of mainstream and sidestream cigarette smoke: nature of the free radicals in gas-phase smoke and in cigarette tar. Environ. Health Perspect. 47, 345–355.
Puzon, G.J., Roberts, A.G., Kramer, D.M., Xun, L., 2005. Formation of soluble Organo−Chromium(III) complexes after chromate reduction in the presence of cellular organics. Environ. Sci. Technol. 39, 2811–2817.
Remucal, C.K., Ginder-Vogel, M., 2014. A critical review of the reactivity of manganese oxides with organic contaminants. Environ. Sci. J. Integr. Environ. Res.: Process. Impacts 16, 1247–1266.
Ruan, X., Sun, Y., Du, W., Tang, Y., Liu, Q., Zhang, Z., et al., 2019. Formation, characteristics, and applications of environmentally persistent free radicals in biochars: a review. Bioresour. Technol. 281, 457–468.
Saravia, J., Lee, G.I., Lomnicki, S., Dellinger, B., Cormier, S.A., 2013. Particulate matter containing environmentally persistent free radicals and adverse infant respiratory health effects: a review. J. Biochem. Mol. Toxicol. 27, 56–68.
Shahane, G., Zipare, K., Pant, R., 2013. Synthesis and characterization of superparamagnetic Fe3O4 nanoparticles for ferrofluid application. Magnetohydrodynamics 49, 317–321.
Shames, A.I., Lev, O., Mikhaylov, A.A., Medvedev, A.G., Gun, J., Prikhodchenko, P.V., 2019. Unusual stabilization of zinc peroxide by manganese oxide: mechanistic understanding by temperature-dependent EPR studies. J. Phys. Chem. C 123, 20884–20892.
Sibera, D., Narkiewicz, U., Guskos, N., Żołnierkiewicz, G., 2009. The preparation and EPR study of nanocrystalline ZnFe2O4. In: Journal of Physics: Conference Series. 146. IOP Publishing, 012014.
Sigmund, G., Santín, C., Pignitter, M., Tepe, N., Doerr, S.H., Hofmann, T., 2021. Environmentally persistent free radicals are ubiquitous in wildfire charcoals and remain stable for years. Communications Earth & Environment 2, 1–6.
Silva, C.V., Aragão, L.E., Barlow, J., Espirito-Santo, F., Young, P.J., Anderson, L.O., et al., 2018. Drought-induced Amazonian wildfires instigate a decadal-scale disruption of forest carbon dynamics. Phil. Trans. Biol. Sci. 373, 20180043.
Stegarescu, A., Lung, I., Leoștean, C., Kacso, I., Opriș, O., Lazăr, M.D., et al., 2020. Green synthesis, characterization and test of MnO2 nanoparticles as catalyst in biofuel production from grape residue and seeds oil. Waste and Biomass Valorization 11, 5003–5013.
Stobbe, E.R., de Boer, B.A., Geus, J.W., 1999. The reduction and oxidation behaviour of manganese oxides. Catal. Today 47, 161–167.
Tong, H., Lakey, P.S., Arangio, A.M., Socorro, J., Kampf, C.J., Berkemeier, T., et al., 2017. Reactive oxygen species formed in aqueous mixtures of secondary organic aerosols and mineral dust influencing cloud chemistry and public health in the Anthropocene. Faraday Discuss 200, 251–270.
United States Department of Agriculture, 2020. Burned-area Report: North Complex. United States Department of Agriculture FOREST SERVICE, p. 14.
Van Der Werf, G.R., Randerson, J.T., Giglio, L., Van Leeuwen, T.T., Chen, Y., Rogers, B. M., et al., 2017. Global fire emissions estimates during 1997–2016. Earth Syst. Sci. Data 9, 697–720.
Van Wieringen, J., 1955. Paramagnetic resonance of divalent manganese incorporated in various lattices. Discuss. Faraday Soc. 19, 118–126.
Vejerano, E.P., Rao, G., Khachatryan, L., Cormier, S.A., Lomnicki, S., 2018. Environmentally persistent free radicals: insights on a new class of pollutants. Environ. Sci. Technol. 52, 2468–2481.
Waggoner, D.C., Wozniak, A.S., Cory, R.M., Hatcher, P.G., 2017. The role of reactive oxygen species in the degradation of lignin derived dissolved organic matter. Geochem. Cosmochim. Acta 208, 171–184.
Wan, X., Li, C., Parikh, S.J., 2021. Chemical composition of soil-associated ash from the southern California Thomas Fire and its potential inhalation risks to farmworkers. J. Environ. Manag. 278, 111570.
Wang, P., Pan, B., Li, H., Huang, Y., Dong, X., Ai, F., et al., 2018. The overlooked occurrence of environmentally persistent free radicals in an area with low-rank coal burning, Xuanwei, China. Environ. Sci. Technol. 52, 1054–1061.
Wang, Z., Wu, L., Zhou, J., Shen, B., Jiang, Z., 2013. Enhanced microwave absorption of Fe3O4 nanocrystals after heterogeneously growing with ZnO nanoshell. RSC Adv. 3, 3309–3315.
Wibbenmeyer, M., McDarris, A., 2021. Wildfires in the United States 101: context and consequences. https://www.rff.org/publications/explainers/wildfires-in-the-united-states-101-context-and-consequences/. (Accessed 29 March 2022).
Williams, A.P., Abatzoglou, J.T., Gershunov, A., Guzman-Morales, J., Bishop, D.A., Balch, J.K., et al., 2019. Observed impacts of anthropogenic climate change on wildfire in California. Earth's Future 7, 892–910.

Williams, A.P., Cook, E.R., Smerdon, J.E., Cook, B.I., Abatzoglou, J.T., Bolles, K., et al., 2020. Large contribution from anthropogenic warming to an emerging North American megadrought. Science 368, 314–318.
Zaunschirm, M., Pignitter, M., Kienesberger, J., Hernler, N., Riegger, C., Eggersdorfer, M., et al., 2018. Contribution of the ratio of tocopherol homologs to the oxidative stability of commercial vegetable oils. Molecules 23, 206.
Zhang, Y., Guo, X., Si, X., Yang, R., Zhou, J., Quan, X., 2019a. Environmentally persistent free radical generation on contaminated soil and their potential biotoxicity to luminous bacteria. Sci. Total Environ. 687, 348–354.
Zhang, Y., Yang, R., Si, X., Duan, X., Quan, X., 2019b. The adverse effect of biochar to aquatic algae- the role of free radicals. Environ. Pollut. 248, 429–437.
Zhu, Y., Wei, J., Liu, Y., Liu, X., Li, J., Zhang, J., 2019. Assessing the effect on the generation of environmentally persistent free radicals in hydrothermal carbonization of sewage sludge. Sci. Rep. 9, 17092.

Update

Chemosphere
Volume 364, Issue , September 2024, Page

DOI: https://doi.org/10.1016/j.chemosphere.2024.143197

Chemosphere 364 (2024) 143197

Contents lists available at ScienceDirect

Chemosphere

journal homepage: www.elsevier.com/locate/chemosphere

Corrigendum

Corrigendum to 'Environmentally persistent free radicals and other paramagnetic species in wildland-urban interface fire ashes' [Chemosphere **363** (2024) 142950]

Mahbub Alam [a], James Sitter [b], Aaron Vannucci [b], Jackson P. Webster [c], Sandrine J. Matiasek [d], Charles N. Alpers [e], Mohammed Baalousha [a,*]

[a] *Center for Environmental Nanoscience and Risk, Department of Environmental Health Sciences, Arnold School of Public Health, University of South Carolina, Columbia, SC, United States*
[b] *Department of Chemistry and Biochemistry, University of South Carolina, Columbia, SC, United States*
[c] *Department of Civil Engineering, California State University Chico, 400 W 1st St, Chico, CA, 95929, United States*
[d] *Department of Earth and Environmental Sciences, California State University Chico, 400 W 1st St, Chico, CA, 95929, United States*
[e] *U.S. Geological Survey, California Water Science Center, 6000 J Street, Sacramento, CA, United States*

In the paper, highlights number 2 and 3 are inaccurate. The revised highlights should read as follows:

1. Paramagnetic species were measured in wildland-urban interface fire ash.
2. The concentrations of EPFRs followed the order: vegetation ash > soil > structural ash > vehicle ash.
3. The concentrations of EPFRs decreased with increased combustion completeness.
4. The concentration of isolated reduced Mn^{2+} ions increased with increased combustion completeness.
5. WUI fire ash may be an important global source of EPFRs and reduced Mn^{2+}-bearing nanomaterials.

Additionally, the Complex and Fire should be capitalized in the keywords as follows:

LNU Lightning Complex Fire.
North Complex Fire.

In the References, the citation for Alam et al., 2023 should have be capitalized.

The authors would like to apologize for any inconvenience caused.

References

Alam, M., Alshehri, T., Wang, J., Singerling, S.A., Alpers, C.N., Baalousha, M., 2023. Identification and quantification of Cr, Cu, and As incidental nanomaterials derived from CCA-treated wood in wildland-urban interface fire ashes. J. Hazard. Mater. 445, 130608.

DOI of original article: https://doi.org/10.1016/j.chemosphere.2024.142950.
* Corresponding author.
E-mail address: mbaalous@mailbox.sc.edu (M. Baalousha).

https://doi.org/10.1016/j.chemosphere.2024.143197

Available online 5 September 2024